CrossMark

ORIGINAL PAPER

Influence of Bedding Angle on Borehole Stability: A Laboratory Investigation of Transverse Isotropic Oil Shale

T. Meier · E. Rybacki · T. Backers · G. Dresen

Abstract The stability of wells drilled into bedded formations, e.g., shales, depends on the orientation between the bedding and the borehole axis. If the borehole is drilled sub-parallel to bedding, the risk of borehole instabilities increases significantly. In this study, we examined the formation of stress-induced borehole breakouts in Posidonia shale by performing a series of thick-walled hollow cylinder experiments with varying orientations of the bedding plane with respect to the borehole axis. The thick-walled hollow cylinders (40 mm in diameter and 80 mm in length containing an 8 mm diameter borehole) were loaded isostatically until formation of breakouts. The onset of borehole breakout development was determined by means of acoustic emission activity, strain measurements, ultrasonic velocities and amplitudes. The critical pressure for breakout initiation decreased from 151 MPa by approximately 65 % as the bedding plane inclination changed from normal to parallel to the borehole axis. The finely bedded structure in the shale resulted in an anisotropy in elasticity and strength from which the variation in strength dominated the integrity of the thick-walled hollow cylinders.

Keywords Borehole stability · Oil shale · Transverse isotropy · Bedding planes · Thick-walled hollow cylinder

T. Meier (✉) · E. Rybacki · G. Dresen
Helmholtz Centre Potsdam, GFZ German Research Centre for Geosciences, Potsdam, Germany
e-mail: Tobias.meier@geomecon.de

T. Meier · T. Backers
Geomecon GmbH, Potsdam, Germany

1 Introduction

An increasing number of wells are being drilled into shale formations because 75 % of all sedimentary basins worldwide contain shale formations (Pei 2008), where shales form the cap rock of conventional oil- and gas reservoirs or in stratigraphic units are used for CO_2 sequestration. More recently, exploitation of shale formations is strongly growing since they are import unconventional oil and gas reservoirs (e.g., Allix et al. 2006; Boyer et al. 2006). Furthermore, shale formations are also potential host rocks for nuclear waste storage, e.g., in Opalinus Clay (Martin and Lanyon 2003) or Boom Clay (Labiouse et al. 2014). However, a number of instability problems are encountered while drilling or excavating shale formations; especially with decreasing angle β between the bedding planes and the borehole axis (Fig. 1), often referred to as 'angle of attack' (Atkinson and Bradford 2002; Gallant et al. 2007; Gazaniol et al. 1995; Khan et al. 2011; Martin and Lanyon 2003; Ottesen 2010; Økland and Cook 1998; Zoback 2010).

The structural heterogeneity of shale is attributed to the orientation distribution of minerals and organic matter, typically resulting in the formation of weak bedding planes (e.g., Chenevert and Gatlin 1965; Gallant et al. 2007) and a pronounced elastic transverse isotropy (TVI) (Dewhurst and Siggins 2006; Johnston and Christensen 1995; Vernik and Liu 1997; Wenk et al. 2008), meaning that properties, e.g., elastic constants and strength properties, parallel to the bedding are isotropic but vary across them (Chong and Smith 1984).

TVI results in an inhomogeneous stress distribution around boreholes that depends on borehole orientation and the orientation of the deviatory stress fields with respect to bedding (Lekhnitskii 1968; Amadei 1983). Several

Fig. 1 a *Top view* of a deformed thick-walled hollow cylinder (PN3) with borehole oriented almost parallel to the bedding planes showing borehole breakouts. **b** Schematic cross-section of the thick-walled hollow cylinder geometry. α is the angle between the normal to the bedding plane and the borehole/specimen axis (Z) and β is referred to as the dip angle. The strike of the bedding planes is oriented parallel to the x-axis direction
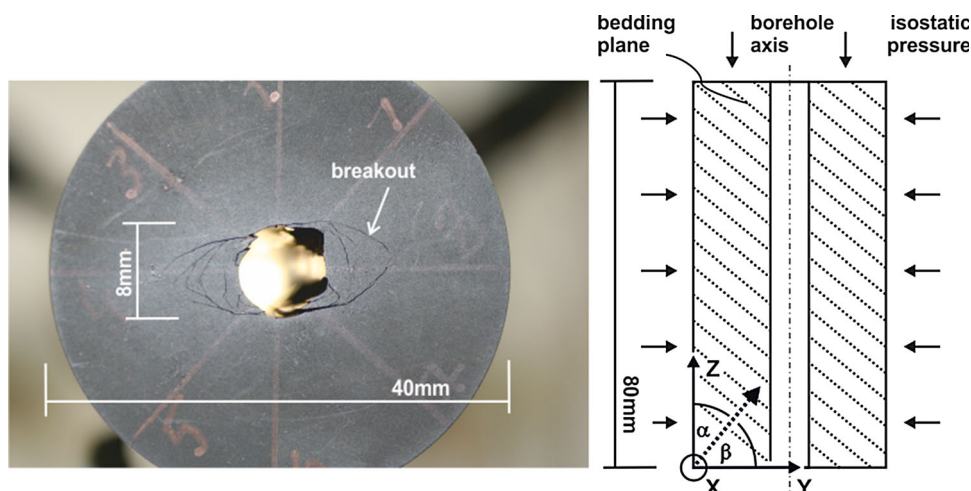
analytical solutions and modeling results exist that predict the stress distribution and borehole collapse or fracture initiation pressures around deviated boreholes in TVI rocks (Aadnoy 1989; Ong and Roegiers 1993, 1996; Gupta and Zaman 1999; Pei 2008). The differences between isotropic and TVI rocks are negligible if the borehole axis is oriented normal to bedding. In this case, the stress field close to the borehole can be calculated from the stress concentration around a hole in an infinite, linear elastic, and isotropic plate (e.g., Zoback 2010). However, neglecting the anisotropy for any other orientation, as commonly done in drilling applications (Gaede et al. 2012; Khan et al. 2011; Birchwood and Noeth 2012), may result in significant errors of stress estimates (Blümling 1986).

In anisotropic rocks bedding plane slip may have a significant effect on borehole and casing stability (Addis et al. 1993; Dusseault et al. 2001; Gazaniol et al. 1995; Økland and Cook 1998; Russell et al. 2003; Skelton et al. 1995; Willson et al. 1999) and has been estimated previously (e.g., Daemen 1983; Gallant et al. 2007; Lee et al. 2012; Vernik and Zoback 1990). However, the considerable effect of elastic anisotropy has been ignored so far in these analyses.

Experimental studies on shale have been done mainly on samples with boreholes drilled either parallel or perpendicular to the bedding (e.g., Aoki 1993; Labiouse and Vietor 2014; Labiouse et al. 2014; Meier et al. 2013). In tests on thick-walled hollow cylinders (TWHC) with bedding planes parallel to the borehole axis Labiouse and Vietor (2014) and Labiouse et al. (2014) observed that breakouts typically initiate at four positions around the borehole wall, leading to a four-lobed breakout pattern in the initial phase of loading. At higher loads, successive buckling failure may occur in direction normal to the bedding (Økland and Cook 1998; Blümling et al. 2007; Labiouse and Vietor 2014). Under isostatic stress conditions and with bedding planes normal to the borehole axis

Meier et al. (2013) showed that breakouts in shales initiated without any preferred orientation. Just a few studies investigated borehole stability of shales with inclined bedding plane orientations. For instance, Økland and Cook (1998) performed TWHC experiments on organic rich Draupne shale from the North Sea and from an outcrop reference shale (J2) to investigate borehole instabilities encountered in highly inclined wells ($\beta < 10°$) drilled in the North Sea. The tests were performed with bedding inclinations of 0°, 10°, 45° and 90°. Experiments conducted on samples with bedding planes parallel to the borehole axis ($\beta = 0°$) resulted in unstable failure at low pressures, whereas tests with $\beta > 80°$ required high pressure to initiate borehole instabilities. Based on these experimental observations, the encountered borehole instability problems in the field were reduced by increasing the 'angle of attack' to >30°, indicating the necessity to study the influence of bedding planes on borehole stability in shales.

Here, we present a series of TWHC experiments on Posidonia shale with varying 'attack' angles between bedding plane and borehole orientation. The laboratory investigations simulated a drill path which deviates from vertical to horizontal through finely bedded shale to study potential changes in failure processes involved in the formation of borehole breakouts. The TWHC experiments are also simulated in a finite element modeling to account for the stress field in the TVI shale.

2 Experimental

2.1 Test Material

Samples were prepared from Posidonia shale cores of the Hills syncline in the Lower Saxony Basin, NW Germany. This Lower Jurassic shale was buried to depths of up to

Table 1 Petrophysical parameters of tested Posidonia shale (Meier et al. 2013)

Maturity	0.88
Porosity (%)	1.1 ± 0.3
Avg. pore throat (nm)	<4.1
Calcite content (wt%)	47.3 ± 0.5
Clay content (wt%)	27.8 ± 1.6
Quartz content (wt%)	17.2 ± 0.4
Pyrite (wt%)	5.3 ± 0.2
Total organic carbon, TOC (wt%)	5.8 ± 0.3
Water content (wt%)	~1

Table 2 Uniaxial compressive strength (UCS) and elastic properties (Young's modulus E, Poisson's ratio v, shear modulus G) of transverse isotropic Posidonia shale

E_{xy}^a	17.3 GPa	E_z^a	10.4 GPa
v_{xy}	0.18	v_{zy}	0.30
G_{xy}	8.9 GPa	G_z	5.5 GPa
UCS_{xy}	75 ± 7 MPa	UCS_z	115 ± 7 MPa
UCS_{45}	60 ± 10 MPa		
n	1.66	v_{yz}	0.17

Values marked with [a] are taken from Meier et al. 2013. Indices xy and z denote parallel and perpendicular to bedding, respectively

~1,800 m before being uplifted to the sub-surface (Mann et al. 1990). The cores, retrieved from a depth interval of 41–51 m, represent a carbonate rich, mature oil shale with a vitrinite reflectance Ro of 0.88 % (Littke et al. 1988). The porosity measured by mercury porosimetry is about 1 %. The dark gray to black samples show fine bedding, defined by calcareous bands of maximum 1 mm thickness and layered organic matter with embedded sub-parallel framboidal pyrite flakes.

The unconfined compressive strength (UCS) parallel to the bedding (index xy) is (35 %) lower than perpendicular to bedding (index z) and distinctly (48 %) lower diagonal to bedding (index 45). Young's moduli are also anisotropic with $E_{xy}/E_z = n \approx 1.7$. Poisson's ratios were found to be $v_{zy} = n \cdot v_{yz}$, where v_{yz} is the Poisson's ratio in opposite loading direction to v_{zy}, being a pre-requisite for transverse isotropic elasticity. The shear modulus normal to bedding can be estimated for oil shales by (Chong and Smith 1984) $G_z = E_{xy}/(1 + n + 2nv_{zy})$ and the shear modulus parallel to the bedding, i.e. in the plane of symmetry, is given by $G_{xy} = E_{xy}/(2 + 2v_{xy})$. Measured petrophysical and geomechanical parameters are given in Tables 1 and 2, respectively.

2.2 Specimen Preparation

Cylindrical specimens were drilled out of the core material under dry conditions with bedding plane orientations α ($90° - \beta$) between 30° and 86° (Fig. 1). The samples were ground to 40 mm diameter and 80 mm length with parallel end surfaces with an accuracy <20 μm. Finally, a central borehole of 8 mm diameter was drilled dry into the sample using a solid carbon drill bit. During preparation of the thick-walled hollow cylinder, dust and drill cuttings were removed by a high-power vacuum cleaner. Specimen dimensions are given in Table 3.

2.3 Experimental Techniques

Each sample was equipped with two pairs of strain gauges and jacketed using 2 mm thin rubber sleeves. Strain gauge signals in circumferential (ε_{circ}) and axial (ε_{ax}) direction were stored with a sampling rate of 2 Hz (HBM MGCplus) with an accuracy of ±3 % at positions parallel and normal to bedding. In addition, twelve acoustic emission (AE) sensors were glued directly onto the sample surface and sealed with epoxy resin. The sensors with a resonant frequency of about 2 MHz were used to record AE and to measure elastic p-wave velocities, (v_p), and elastic p-wave amplitudes in axial and radial direction. Transducer signals were amplified by 60 dB using a pre-amplifier equipped with a 100 kHz high-pass filter (Physical Acoustic Corporation). AE's and ultrasonic waveforms were stored using a 16 channel transient recording system (DaxBox, Prökel GmbH) with an amplitude resolution of 16 bit at 10 MHz sampling rate. All experiments have been performed in a stiff, servo-controlled loading frame (MTS), equipped with a 200 MPa confining pressure vessel. For non-destructive visualization of fractures within deformed samples, we used an X-ray computer tomography system (X-ray CT, Phoenix X-Ray nanotom 180NF) with an operation voltage of ≈ 150 kV under ambient pressure conditions. Resolution of the scans varied between 22 and 40 μm per voxel.

Subsequently, the microstructures were analyzed on thin sections prepared normal to the borehole axis using a scanning electron microscope (SEM, Carl Zeiss SMT-Ultra 55 Plus) in normal and backscattered scanning electron mode.

2.4 Experimental Procedure

A total of six thick-walled hollow cylinders with $30° \leq \alpha \leq 86°$ were loaded by increasing the isostatic pressure at a rate of 1–2 MPa/min until formation of borehole breakouts. The borehole was kept at atmospheric pressure. For each sample, axial and radial strain, AE activity, ultrasonic p-wave velocity and amplitudes were recorded to detect breakout initiation. Unloading of samples was performed at a rate of 2–4 MPa/min.

Table 3 Specimen geometry, loading rate and critical isostatic confining pressures for borehole breakout formation estimated from the onset of AE activity (P_{AE}), ultrasonic amplitude (P_{amp}), ultrasonic velocity (P_{vp}), and circumferential strain (P_ε)

Sample name	b (mm)	l (mm)	a (mm)	α (°)	Rate (MPa/min)	P_{AE} (MPa)	P_{amp} (MPa)	P_{vp} (MPa)	P_ε (MPa)	P* (MPa)
PN1	40	80	6	0	1	138	170	160	159	157 ± 10
PN2	50	80	10	0	0.5	130	–	144	144	140 ± 4
PN*	50	80	8	0	–	–	–	–	–	151 ± 5
PN3	40	80	8	86.4 ± 0.4	0.5	49	53	54	52	52 ± 2
PN4	40	80	8	78.4 ± 0.9	2	–	62	61	59	61 ± 2
PN5	40	80	8	73.3 ± 2.8	1	–	62	62	53	59 ± 8
PN6	40	80	8	63.0 ± 0.5	1	–	82	79	76	79 ± 3
PN7	40	80	8	53.6 ± 1.1	1	–	88	88	86	87 ± 5
PN8	40	80	8	30 ± 2.0	1	126	–	–	–	126–10

b is specimen diameter, l specimen height, a borehole diameter, and α is dipping angle, PN* is interpolated between PN1 and PN2 using the data from Meier et al. (2013)

3 Results

3.1 Borehole Breakout Initiation Pressures

3.1.1 Ultrasonic Velocities, Amplitudes and Acoustic Emission Measurements

Generally, the measured v_p of the specimens increased with increasing confining pressure. Differences of v_p are related to the bedding plane orientation. Measurements parallel to bedding exhibited the highest velocities (4.0 ± 0.3 km/s at 0.1 MPa pressure), whereas the lowest velocities (3.4 ± 0.2 km/s at 0.1 MPa pressure) were recorded normal to bedding. Intermediate velocities were measured along traces inclined 45° to the bedding (Fig. 2a).

Measurements non-parallel to the bedding planes showed a distinct drop of v_p upon reaching a certain pressure, which is interpreted as the onset of breakout formation, P_{vp}. Measured ultrasonic amplitudes followed the same behavior as the measured v_p but difference in magnitude could not be related to the bedding plane orientation. However, at a certain pressure, P_{amp}, we observed a marked drop in amplitudes, which sets the onset of borehole breakouts.

Due to the low amount of strong minerals (quartz, pyrite) in the investigated shales, AE's were rarely observed during loading, in contrast to sandstones loaded under similar conditions (e.g., Dresen et al. 2010; Papamichos et al. 2010). If present, the AE hypocenters were located close to the borehole with an estimated location
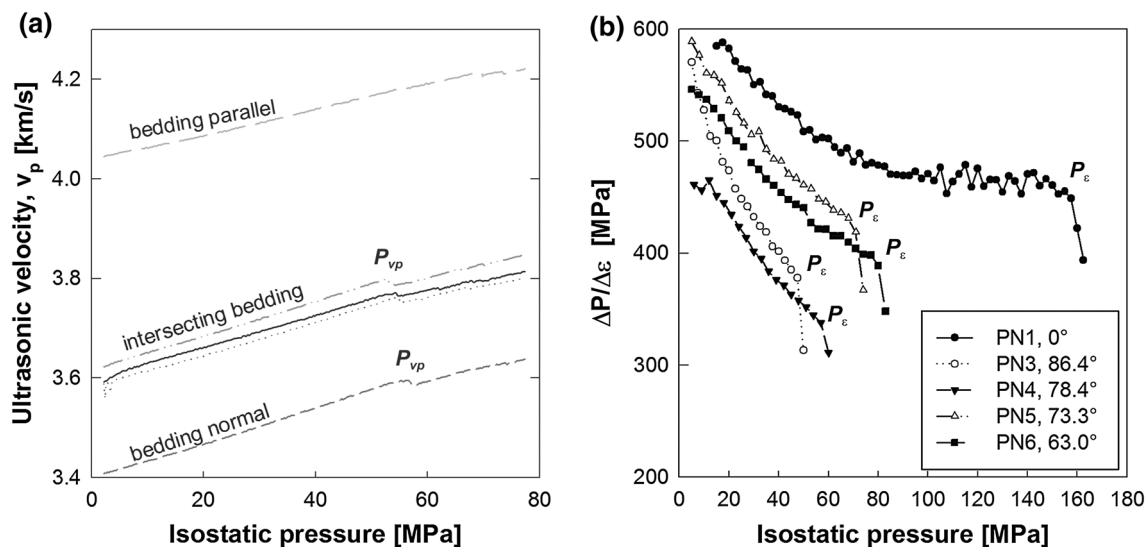
Fig. 2 **a** Radial ultrasonic velocities versus isostatic pressure measured for specimen PN3. P_{vp} in the curves indicate the onset of borehole breakouts. **b** Derivative of isostatic pressure changes with change of the associated circumferential strain versus isostatic pressure. P_ε marks the onset of breakout development

error of ± 3 mm. A distinct onset or increase in AE activity, indicating breakout nucleation at pressure P_{AE}, was observed only in two experiments (see Table 3).

3.1.2 Strain Measurements

Figure 2b shows the development of $\Delta P/\Delta\varepsilon_{circ}$ versus P. $\Delta\varepsilon_{circ}$ was measured parallel to the strike of the bedding except sample PN5, where $\Delta\varepsilon_{circ}$ was measured normal to the strike of the bedding. The curves depict initially a continuous, almost linear decrease with increasing pressure. At elevated pressures the samples showed a non-linear compaction behavior, probably due to the formation of inelastic crack damage at the borehole indicating the formation of borehole breakouts at a critical pressure, P_ε, which depends on the bedding orientation. Beyond P_ε the curve dropped significantly during sample compaction, indicating further inelastic deformation of the borehole.

3.1.3 Critical Borehole Breakout Initiation Pressures

The average critical isostatic pressure required for breakout nucleation, P^*, is given in Table 3, based on strain, AE activity, and ultrasonic p-wave data. For sample PN8, only AE activity was recorded during loading up to 133 MPa pressure. Here, we used additional X-ray CT scans of the deformed specimen after unloading, which showed initial breakout formation. The critical pressure at breakout initiation depends on borehole orientation with respect to bedding as shown in Fig. 3. P^* decreased almost linearly by 65 % from ~ 151 MPa at $\alpha = 0°$ (normal to bedding) to ~ 52 MPa at $\alpha = 86.4°$ (almost parallel to bedding). Note that the borehole diameters of samples PN1 and PN2 were
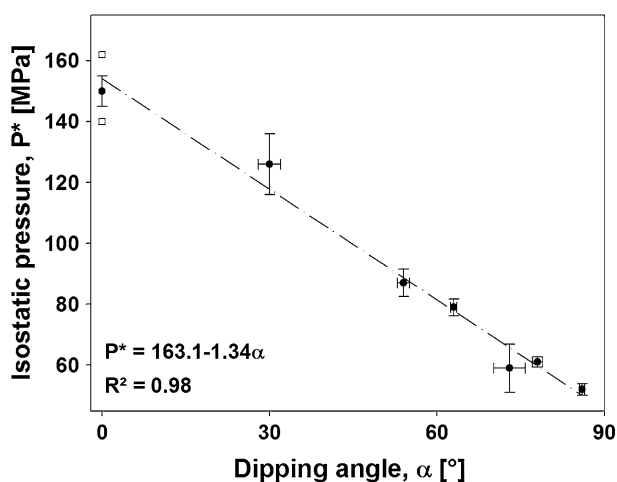
6 and 10 mm, respectively. Interpolation of P^* between PN1 and PN2 gave $P^* = 151$ MPa for a borehole diameter of 8 mm for $\alpha = 0°$ (PN1 and PN2 taken from Meier et al. 2013). The decrease of P^* for thick-walled hollow Posidonia shale cylinders with increasing angle α can be approximated by a linear equation of the form P^* [MPa] $= 163.1$ [MPa] $- 1.34\alpha$ [°] ($R^2 = 0.98$).

3.2 Microstructural Observations

Based on microstructural investigations, initial failure seemed to be always related to slip on bedding planes, leading to a four-lobed breakout pattern. Further loading beyond breakout initiation triggered shear or buckling failure depending on the bedding plane dip (Fig. 4).

3.2.1 Breakout Formation in Boreholes Oriented Sub-parallel to Bedding

For specimens with bedding planes intersecting the borehole axis at angles of $63° < \alpha < 86°$, failure initiated at the borehole wall where the bedding planes are expected to be favorably orientated for shear failure, i.e. $20°$–$45°$ to the strike of the bedding (Figs. 4, 5). During loading beyond P^*, small, crescent-shaped fragments were ejected into the borehole resulting in nearly rectangular cross sections as also observed in soft clays (e.g., Labiouse and Vietor 2014).
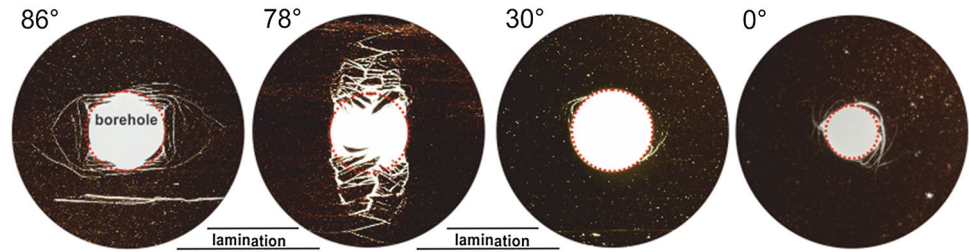
Sample PN4 was loaded 25 MPa beyond the breakout initiation pressure causing intense crack damage (Fig. 4). The X-ray CT images (Fig. 5) indicate that the progressive crack damage occurred by separation of the rock material into blocky fragments of 0.5-3 mm thickness normal to bedding. These are subjected to bending and increasing tangential stress eventually leading to buckling failure. Breakout propagation appears to be normal to the strike of the bedding planes.

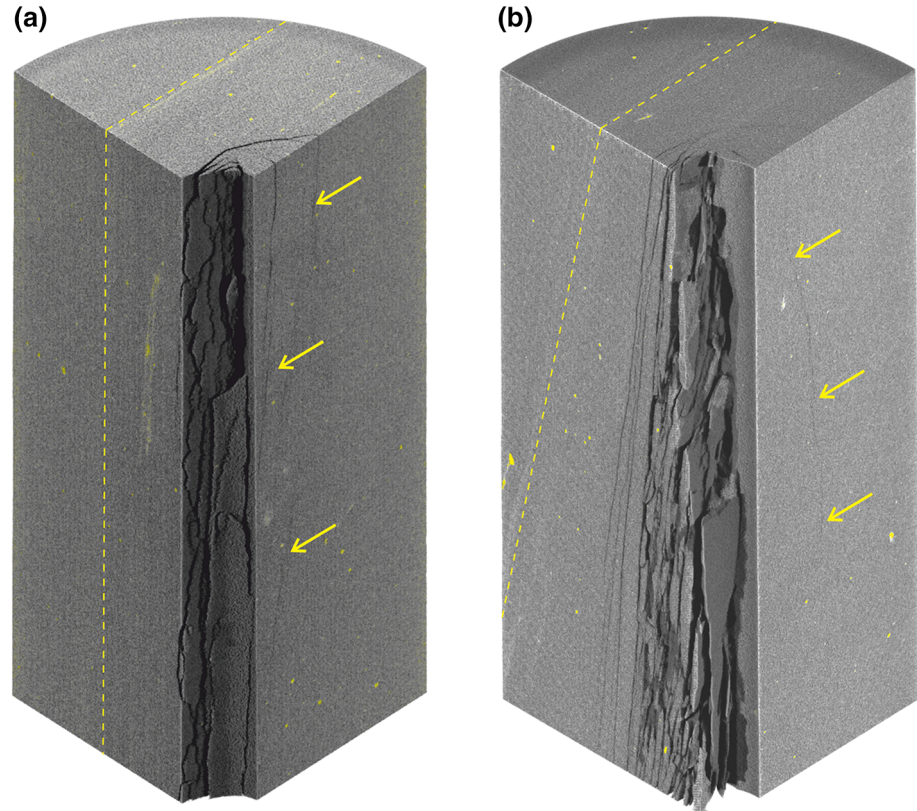### 3.2.2 Wellbore Damage in Boreholes Oriented Normal to Bedding

For samples with bedding planes oriented normal to the borehole axis, i.e., $\alpha \approx 0°$, spiral-shaped shear fractures developed around the borehole. This fracture pattern in Posidonia Shale can be successfully modeled using the Mohr–Coulomb failure criterion (Meier et al. 2013). The observed breakout depth varied along the borehole axis, possibly related to material heterogeneities such as different clay content, clastic minerals and porosity.

For $30° < \alpha < 63°$, fractures initiated at about $45°$ to the strike of the bedding. The fractures propagated along the bedding planes but reoriented into a borehole tangential direction at some distance from the borehole, revealing a

Fig. 3 Decrease of the critical pressure P^* for borehole breakout initiation with increasing dip angle α. Note that specimens PN1 and PN2 ($\alpha = 0°$, *open squares*) have different borehole diameters (6, 10 mm) compared to the remaining samples (8 mm)

double-lobed breakout pattern. Along the borehole wall the fractures followed the bedding planes (Fig. 6).

4 Discussion

To explain the influence of the dip angle on stress-induced borehole breakouts in shales, we consider the contributions of elastic and strength anisotropy. The elastic anisotropy is caused mainly by the variations of porosity, organic material and mineral composition between layers of the shale matrix. In contrast, the anisotropy of strength parameters is mainly associated with the existence of weak bedding planes. In the following, we use finite element modeling to analyze the effect of elastic anisotropy on the stress field in a transverse isotropic TWHC with varying bedding plane orientation subjected to isostatic loading.

The determined stress field is then used to evaluate the stresses operating on the bedding planes. From this analysis, the width of potential failure regions around the borehole wall is estimated for different bedding plane orientations and compared to models based on isotropic material behavior.

4.1 Stress Field in a Transverse Thick-walled Hollow Cylinder

One quarter of the cylindrical specimens of 40 mm diameter and 80 mm height were meshed using a commercial finite element (FE) code (Comsol Multiphysics). The mesh size was fourfold refined by an arithmetic sequence toward the 8 mm borehole (Fig. 7a). The borehole perimeter was divided into 12 radial segments and 80 segments along its height. In total, the mesh consisted of 11,520 hexahedra.

Fig. 6 X-ray CT scans showing one quarter of specimens **a** PN7 and **b** PN6 with $\alpha = 53°$ and $63°$, respectively. The bedding plane orientation is highlighted by *yellow lines*. Note that dip angles of the bedding are different, producing different breakout patterns (color figure online)
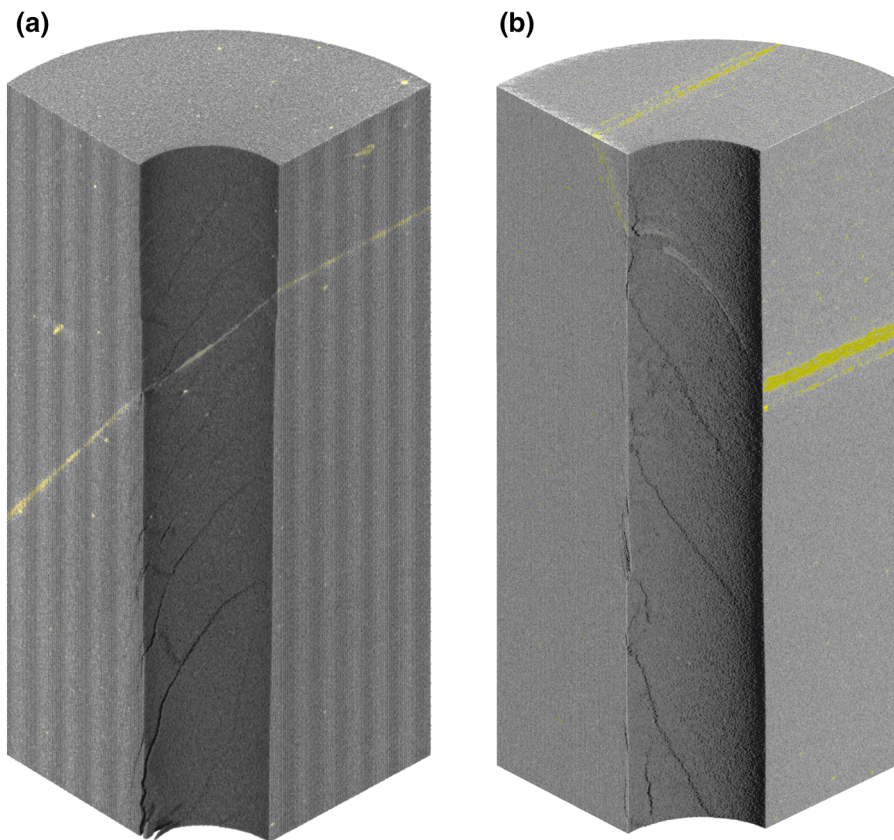
To model the stress distribution prior to failure, we assumed a linear elastic material behavior using the parameters listed in Table 2. The isostatic load was applied to the mantle and top surface of the cylinder, whereas the bottom surface was fixed with zero displacement in vertical direction (along the z-axis) and without kinematic constraints in the XY-plane. The borehole wall was defined as a pressure-free boundary.

In the simulation, the coordinate system of the applied isostatic stress field coincided with the coordinate system of the TWHC (X, Y, Z). In contrast, the coordinate system of the material properties was rotated around the x-axis by different angles α in order to simulate the varying dip of the bedding planes with respect to the borehole axis. Hence, the strike of the lamination was always in X-direction. For each point in the FE model, the full stress tensor was obtained in the X, Y, Z coordinate system from which the tangential $\sigma_{\theta\theta}$, radial σ_{rr}, and vertical stress σ_{zz} are determined by

$$\sigma_{\theta\theta} = \frac{1}{2}(\sigma_{XX} + \sigma_{YY}) - \frac{1}{2}(\sigma_{XX} - \sigma_{YY})\cos 2\theta - \sigma_{XY}\sin 2\theta \tag{1}$$

$$\sigma_{rr} = \frac{1}{2}(\sigma_{XX} + \sigma_{YY}) + \frac{1}{2}(\sigma_{XX} - \sigma_{YY})\cos 2\theta + \sigma_{XY}\sin 2\theta \tag{2}$$

$$\sigma_{zz} = \sigma_{ZZ} \tag{3}$$

where θ is the positive angle measured counterclockwise from the x-axis toward the y-axis (see Fig. 7a).

Figure 7b and c shows the tangential and vertical stress distributions versus θ at the borehole wall, normalized to the critical isostatic pressure P^* for breakout initiation for the bedding dip angles measured in our experiments. At the borehole wall the radial stresses are equal to zero due to the pressure-free borehole and are not shown.

In case of bedding planes oriented normal to the borehole axis ($\alpha = 0°$), a radial symmetric stress distribution is achieved due to isotropic material properties in radial direction. This result is consistent with analytical solutions for TWHCs based on linear elastic and isotropic material behavior (e.g., Jaeger et al. 2007).

In case of bedding planes inclined to the borehole axis ($\alpha \neq 0°$) the model predicts two local tangential stress maxima and one minimum, which progressively increase in magnitude with increasing bedding plane inclination (Fig. 7b). These stress distributions are in agreement with analytical solutions for linear elastic and transverse isotropic material behavior (e.g., Aadnoy 1989). At a dip angle of $\alpha = 86°$ (PN3), the ratio $\sigma_{\theta\theta}/P^*$ varies from 2.01 ($\theta = 45°$) to 2.18 ($\theta = 90°$), which corresponds to a maximum change of about 4.6 % in tangential stress
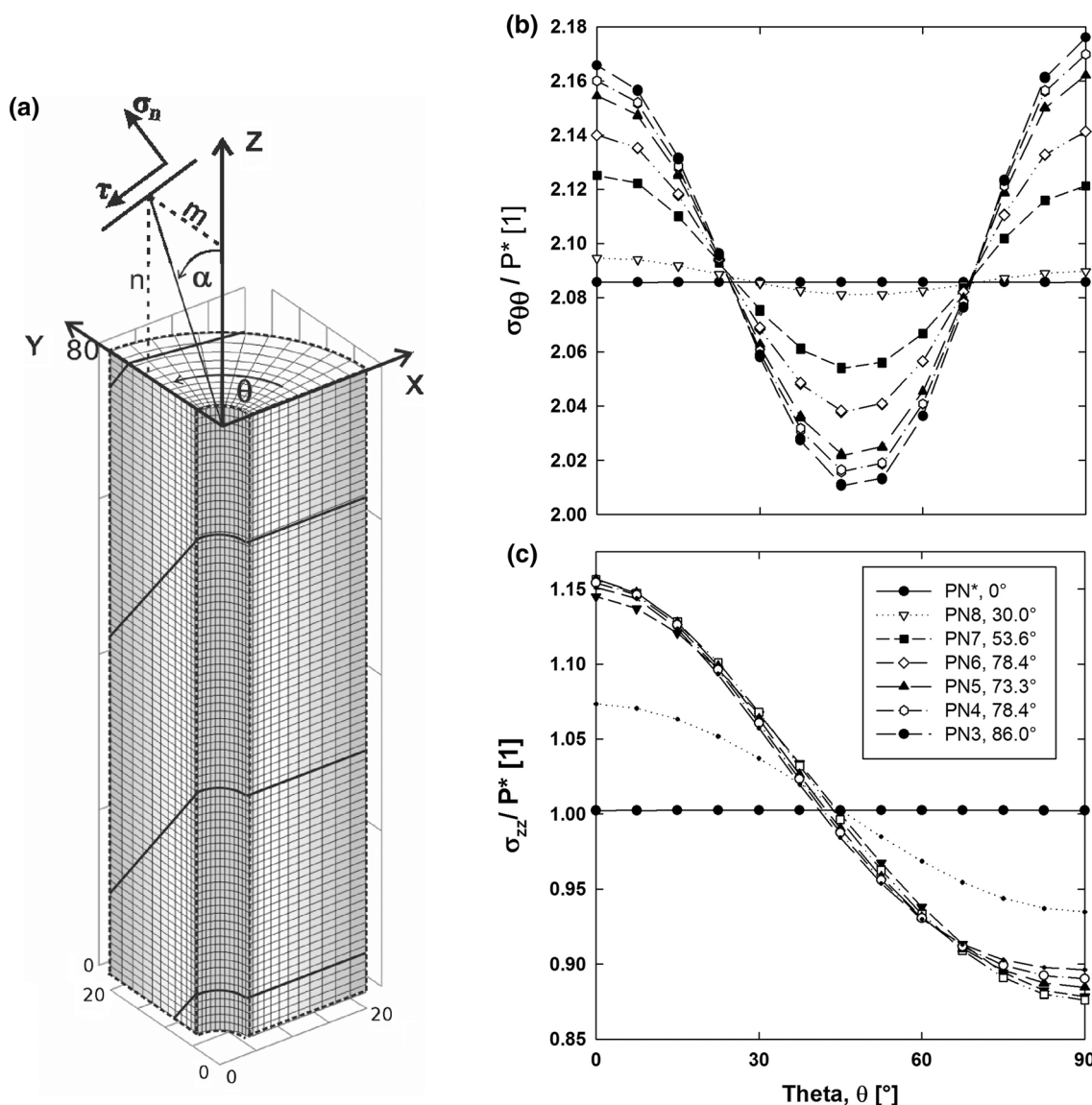
Fig. 7 a FEM mesh consisting of 11,520 hexahedra with bedding plane orientation represented by *thick black lines*. **b** Normalized tangential stress and **c** vertical stress at the borehole wall for different bedding plane orientations α versus azimuth angle θ between strike of bedding planes and stress direction

compared to isotropic material ($\sigma_{\theta\theta}/P^* = 2.08$). It is interesting to note that the vertical stress changes with dipping angle as shown in Fig. 7c. However, compared to the experimental data the change in tangential and vertical stress is too small to explain the observed decrease in the breakout initiation pressure of the shale samples of about 65 % with increasing dip angle.

4.2 Stress Acting on Inclined Bedding Planes

Microstructural observations suggest that for $\alpha \neq 0°$ failure at the borehole wall is localized at the bedding planes acting as planar weak zones. Therefore, we assume that the nucleation of borehole breakouts occurs if the shear stress parallel to bedding exceeds a critical value that initiates local slip.

Shear stress, τ, and normal stress, σ_n, operating on bedding planes with varying orientation can be expressed by (Jaeger et al. 2007)

$$\sigma_n = \sigma_{XX}l^2 + \sigma_{YY}m^2 + \sigma_{ZZ}n^2 + 2(\sigma_{XY}lm + \sigma_{YZ}mn + \sigma_{XZ}nl) \tag{4}$$

where l, m, n are the direction cosines of the normal to the plane. For a TWHC with the strike of the bedding parallel

$$\tau = \sqrt{(\sigma_{XX}l + \sigma_{XY}m + \sigma_{XZ}n)^2 + (\sigma_{XY}l + \sigma_{YY}m + \sigma_{YZ}n)^2 + (\sigma_{XZ}l + \sigma_{YZ}m + \sigma_{ZZ}n)^2 - \sigma_n^2} \qquad (5)$$

to the x-axis (see Fig. 7a), the direction cosines between the axis of the borehole and the normal to the bedding plane are given by

$$l = \sqrt{1 - \cos(90° - \alpha)^2 - \cos(\alpha)^2} = 0,$$
$$m = \cos(90° - \alpha),$$
$$n = \cos(\alpha)$$

Inserting l, m, n into Eq. 4 and 5 yields

$$\sigma_n = \sigma_{YY}m^2 + \sigma_{ZZ}n^2 + 2\sigma_{YZ}mn \qquad (6)$$

$$\tau = \sqrt{(\sigma_{XY}m + \sigma_{XZ}n)^2 + (\sigma_{YY}m + \sigma_{YZ}n)^2 + (\sigma_{YZ}m + \sigma_{ZZ}n)^2 - \sigma_n^2} \qquad (7)$$

Based on these relationships and accounting for the stress field of the transverse isotropic shale cylinder, we calculated the shear and normal stress acting on the weak bedding planes. As shown in Fig. 8a and b, the shear stress reaches a maximum at an angle of $\theta = 45°$ whereas the normal stress decreases monotonically with increasing θ. The shear and normal stress for a TWHC with bedding planes normal to the borehole axis (e.g., PN1 in Fig. 8 a, and b) yields zero and the vertical stress, respectively.

In most experiments performed on specimens with bedding inclined to the borehole axis, initial failure occurred at θ between 20° to 30° (PN3 to PN5). Assuming that failure along bedding planes occurred for most tests at an average $\theta = 25° \pm 5°$ we can estimate the cohesion and friction coefficient by applying a linear Mohr–Coulomb failure criterion. Using the calculated shear and normal stresses at $\theta = 25°$ (vertical lines in Fig. 8a, b), the estimated friction coefficient μ_w is 0.37 (friction angle 20.3°) and the cohesion C_w is 9.6 MPa for bedding plane slip in Posidonia shale. Note, that samples with $\alpha = 0°$ are not taken into account here since bedding plane slip is not possible. The estimated friction coefficient and cohesion for the weak bedding planes are distinctly lower than the cohesion and friction coefficient determined for triaxial compression of intact Posidonia shale specimens cored normal to bedding, i.e. $\alpha = 0°$ (pers. comm. M. Makasi, Fig. 9).

The effect of weak bedding planes on potential failure regions around the borehole is illustrated in Fig. 10 using the results of the numerical simulations and accounting for the difference between isotropic and TVI material. For low inclination angles broad to double-lobed failure regions form whereas distinct four-lobed breakouts develop for high bedding plane inclinations. Variations in failure
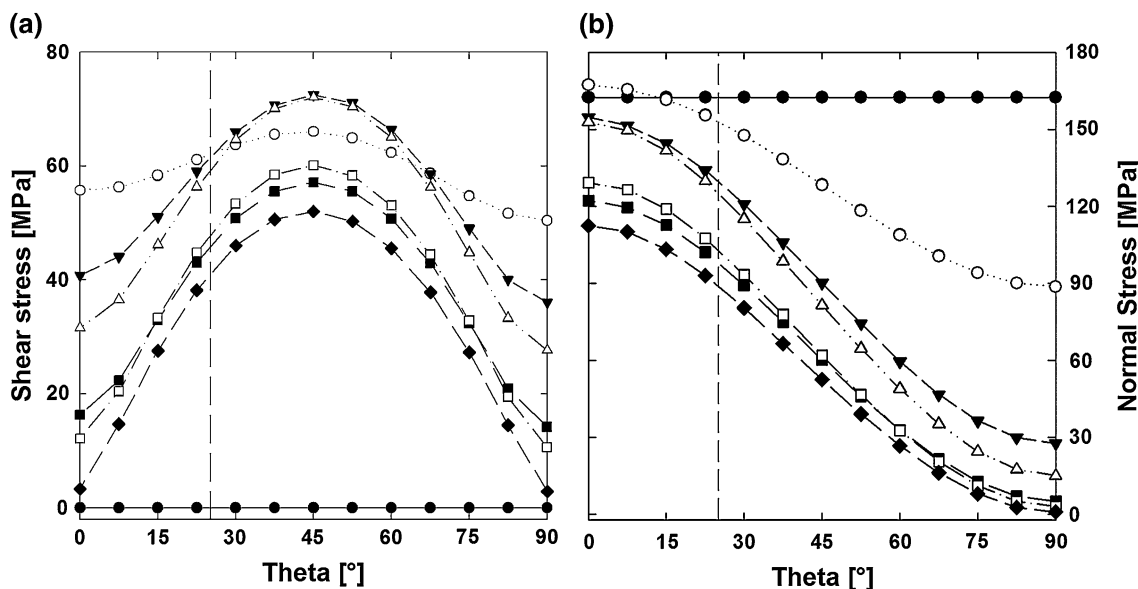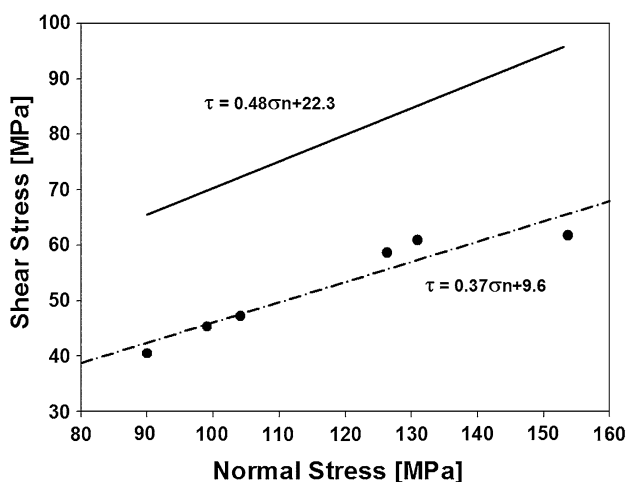

Fig. 8 a Shear stress, and b normal stress along the borehole periphery. *Dashed lines* indicate $\theta = 25°$

Fig. 9 Modeled shear versus normal stress for breakout initiation of samples PN3 to PN8. *Solid line* represents the Mohr–Coulomb failure criterion of intact Posidonia shale tested normal to bedding (pers. comm. M. Makasi)

patterns between isotropic and TVI material are negligible as expected from the relatively small differences in tangential and vertical stress between isotropic and TVI material behavior (see Fig. 7b, c). However, the modeled slip zones are in good agreement with the observed initial failure patterns, in particular at large dip angles.

4.3 Comparison to Another Approach for Predicting Failure of Rocks Containing Weak Bedding Planes

Vernik and Zoback (1990) proposed a model to predict borehole breakouts in isotropic rocks containing weak bedding planes with different dipping angles. Using the Mohr–Coulomb failure criterion the strength of those rocks can be described by

$$S_1 = S_3 + \frac{2(S_w + \mu_w S_3)}{(1 - \mu_w \cot \theta) \sin 2\theta} \tag{8}$$

where θ is the angle between the maximum principle stress S_1 and the normal to the bedding plane and S_w is the intrinsic shear strength, which is given by

$$S_w = 2C_w \left(\sqrt{\mu_w^2 + 1} + \mu_w \right) \tag{9}$$

For a pressure-free borehole with $S_3 = \sigma_{rr} = 0$ and $S_1 = \sigma_{\theta\theta}$ Eq. 9 and 10 can be re-written as

$$\sigma_{\theta\theta,f} = \frac{4C_w \left(\sqrt{\mu_w^2 + 1} + \mu_w \right)}{(1 - \mu_w \cot \theta) \sin 2\theta} \tag{10}$$

which yields the maximum tangential stress the bedding planes can sustain and borehole failure along bedding planes is anticipated in case $\sigma_{\theta\theta} > \sigma_{\theta\theta,f}$. If the strength of the intact rock is lower than $\sigma_{\theta\theta,f}$ for some arbitrary θ, failure for the intact rock is anticipated in case $\sigma_{\theta\theta} > \mathrm{UCS}$. This failure criterion is of a shoulder-type form predicting equal strength parallel and normal to the bedding and a reduced strength in between, which may be applicable for some isotropic rocks containing weak bedding planes (Donath 1961), but does not seem to fit TVI rocks (Pei 2008), where the strength normal to bedding is larger than parallel to bedding. We, therefore, adjusted the criterion to fit the strength of Posidonia shale based on the measured UCS (Table 2) using UCS_z for the strength normal to bedding (large θ) and UCS_{xy} for the strength parallel to the bedding (small θ). Figure 11 shows the predicted strength of Posidonia shale around the borehole for different cohesions values. For a slightly reduced C_w of 7 MPa compared to 9.6 MPa as obtained from the TWHC test, the measured UCS at 45° can be adequately fitted. Failure patterns predicted by this failure criterion for the TWHC experiment (PN3) with bedding plane sub-parallel to the borehole axis are shown in Fig. 11 (inset), being in good agreement to the observed failure patterns
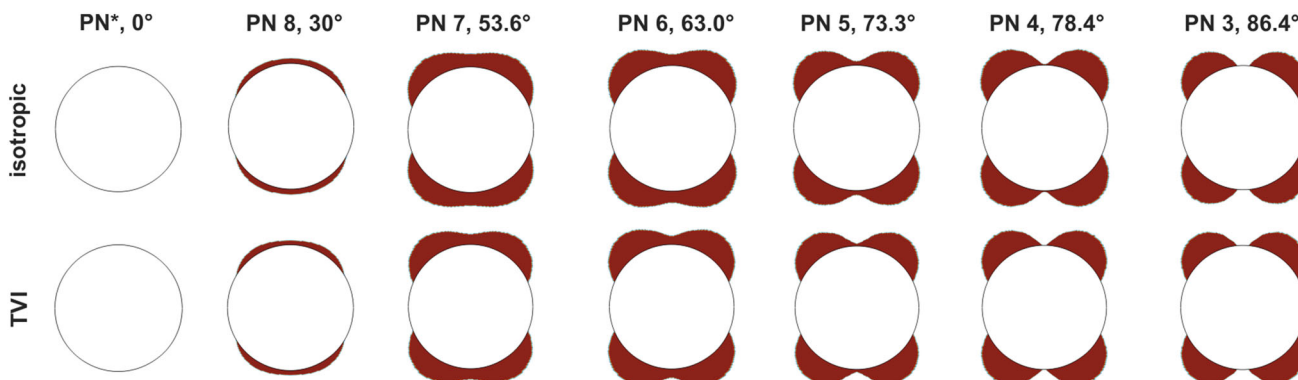
Fig. 10 Modeled breakout pattern around the borehole for different bedding plane inclination angles in isotropic rock (*top*) and TVI rock (*bottom*)
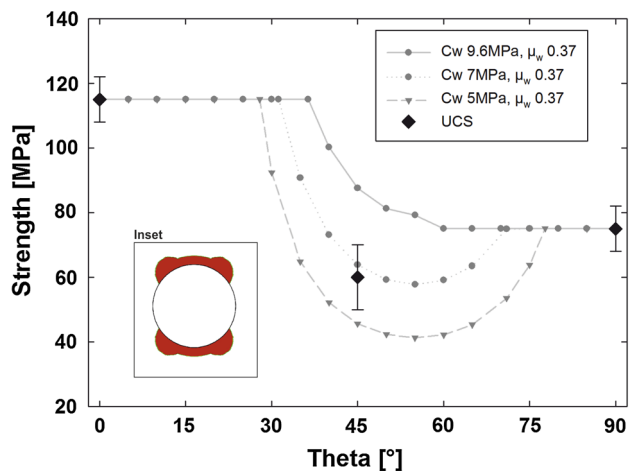
Fig. 11 Strength around one quarter of a borehole and predicted breakout pattern based on a modified failure criterion proposed by Vernik and Zoback (1990). Bedding plane strike is at $\theta = 0°$

5 Conclusions

The observed initial failure was due to slip along bedding planes. This initial failure being a starting point for more severe breakouts forming either as shear or buckling failure. The latter failure process occurred particularly in boreholes sub- to parallel to the bedding planes, which needed the lowest stresses to induce borehole breakouts. This is in close agreement with documentations of borehole instabilities drilled in bedded formations.

Numerical modeling of the stress field in the thick-walled hollow cylinder showed that, depending on the bedding plane inclination, the stress field varies up to 4.6 % from isotropic solutions. This stress anisotropy induced by the anisotropy of the elastic constants is minor and negligible in comparison to the strength anisotropy of the rock. Borehole integrity in the tested Posidonia shale is, hence, depending on the strength of bedding planes.

The strength of the weak bedding planes, in terms of cohesion and friction coefficient, could be determined by resolving the shear and normal stress on the weak bedding planes at the onset of breakout initiation. The determined strength parameters were then used to successfully predict the observed breakout patterns at the beginning of breakout development. Furthermore, the model of Vernik and Zoback (1990) was modified and applied to successfully on shales.

References

Aadnoy BS (1989) Stresses around horizontal boreholes drilled in sedimentary rocks. J Pet Sci Eng 2: 349–360. Retrieved from http://www.sciencedirect.com/science/article/pii/0920410589900090

Addis T, Last N, Boulter D, Roca-ramisa L, Plumb D (1993) The quest for borehole stability in the Cusiana field, Colombia. Oilfield Rev 33–43

Allix P, Burnham A, Fowler T, Herron M, Kleinberg R., Symington B (2006) Coaxing oil from shale. Oilfield Rev Winter 4–15

Amadei B (1983) Lecture notes in engineering, 2 series volume: rock anisotropy and the theory of stress measurements. Springer, Berlin Heidelberg

Aoki, T, Tan C P, Bamford W E (1993) Effects of deformation and strength anisotropy on borehole failure in saturated shales. Int J Rock Mech Min Sci Geomech Abstr 30(7): 1031–1034. Retrieved from http://cat.inist.fr/?aModele=afficheNandcpsidt=3892518

Atkinson C, Bradford I (2002) Effect of inhomogeneous rock properties on the stability of wellbores. In: Karihaloo BL (ed) IUTAM symposium on analytical and computational fracture mechanics of non-homogeneous material. Kluwer Academic Publishers, pp 95–104

Birchwood R, Noeth S (2012) Horizontal stress contrast in the shallow marine sediments of the Gulf of Mexico sites Walker Ridge 313 and Atwater Valley 13 and 14—geological observations, effects on wellbore stability, and implications for drilling. Mar Pet Geol 34(1):186–208. doi:10.1016/j.marpetgeo.2012.01.008

Blümling (1986) In-situ-Spannungsmessung in Tiefbohrungen mit Hilfe von Bohrlochrandausbrüchen und die Spannungsverteilung in der Kruste Mitteleuropas und Australiens. Doctoral dissertation. University of Karlsruhe

Blümling P, Bernier F, Lebon P, Martin CD (2007) The excavation damaged zone in clay formations time-dependent behaviour and influence on performance assessment. Phys Chem Earth Parts A/B/C 32(8–14):588–599. doi:10.1016/j.pce.2006.04.034

Boyer C, Kieschnick J, Suarez-Rivera R, Lewis RE, Waters G (2006) Producing gas from its source. Oilfield Rev, Autumn, pp 36–49

Chenevert ME, Gatlin C (1965) Mechanical anisotropies of laminated sedimentary rocks. SPE J 890-PA 5(1):67–77. doi:10.2118/890-PA

Chong K, Smith J (1984) Mechanics of oil shale. Spoon Press, Prague

Daemen JJK (1983) Slip zones for discontinuities parallel to circular tunnels or shafts. Int J Rock Mech Mining Sci Geomech Abstr 20(3):135–148. doi:10.1016/0148-9062(83)91303-7

Dewhurst DN, Siggins AF (2006) Impact of fabric, microcracks and stress field on shale anisotropy. Geophys J Int 165(1):135–148. doi:10.1111/j.1365-246X.2006.02834.x

Donath FA (1961) Experimental study of shear failure in anisotropic rocks. Geol Soc Am Bull 72:985–990

Dresen G, Stanchits S, Rybacki E (2010) Borehole breakout evolution through acoustic emission location analysis. Int J Rock Mech Min Sci 47(3):426–435. doi:10.1016/j.ijrmms.2009.12.010

Dusseault MB, Bruno MS, Barrera J (2001) Casing shear: causes, cases, cures. In: SPE international. Oil and gas conference and exhibition, pp 98–107

Gaede O, Karpfinger F, Jocker J, Prioul R (2012) Comparison between analytical and 3D finite element solutions for borehole stresses in anisotropic elastic rock. Int J Rock Mech Min Sci 51:53–63. doi:10.1016/j.ijrmms.2011.12.010

Gallant C, Zhang J, Wolfe C A, Freemann J, Al-Bazali T, Reese M (2007) Wellbore stability considerations for drilling high-angle wells through finely laminated shale: a case study from Terra Nova. SPE 110742-MS

Gazaniol D, Forsans T, Boisson MJF, Piau J-M (1995) Wellbore failure mechanisms in shales: prediction and prevention. J Pet Technol 47(7): 589–595. Retrieved from http://www.onepetro.org/mslib/servlet/onepetropreview?id=00028851

Gupta D, Zaman M (1999) Stability of boreholes in a geologic medium including the effects of anisotropy. Appl Math Mech 20(8):837–866

Jaeger JC, Cook NGW, Zimmerman RW (2007) Fundamentals of rock mechanics. Imaging, 4th edn. Blackwell, Oxford

Johnston JE, Christensen NI (1995) Seismic anisotropy of shales. J Geophys Res 100 (B4): 5991–6003. Retrieved from http://www.agu.org/pubs/crossref/1995/95JB00031.shtml

Khan S, Ansari S, Han H, Khosravi N (2011) Importance of shale anisotropy in estimating in-situ stresses and wellbore stability analysis in Horn River basin. SPE Int CSUG/SPE. Retrieved from http://www.onepetro.org/mslib/servlet/onepetropreview?id=SPE-149433-MS

Labiouse V, Vietor T (2014) Laboratory and in situ simulation tests of the excavation damaged zone around galleries in opalinus clay. Rock Mech Rock Eng 47(1):57–70

Labiouse V, Sauthier C, You S (2014) Hollow cylinder simulation experiments of galleries in Boom Clay formation. Rock Mech Rock Eng 47(1):43–55

Lee H, Ong SH, Azeemuddin M, Goodman H (2012) A wellbore stability model for formations with anisotropic rock strengths. J Pet Sci Eng 96–97:109–119. doi:10.1016/j.petrol.2012.08.010

Lekhnitskii (1968) Anisotropic plates. Gordon and Breach Science Publishers, Philadelphia

Littke R, Baker DR, Leythaeuser D (1988) Microscopic and sedimentologic evidence for the generation and migration of hydrocarbons in Toarcian source rocks of different maturities. Org Geochem 13(1–3):549–559

Mann U, Düppendecker S, Langen A, Ropertz B, Welte DH (1990) Pore network evolution of the lower toarcian posidonian shale during petroleum generation and expulsion—a multidisciplinary approach. Zbl Geologische Paläontologie Teil I 8:1051–1071

Martin CD, Lanyon GW (2003) Measurement of in situ stress in weak rocks at Mont Terri Rock Laboratory, Switzerland. Int J Rock Mech Min Sci 40(7–8):1077–1088. doi:10.1016/S1365-1609(03)00113-8

Meier T, Rybacki E, Reinicke A, Dresen G (2013) Influence of borehole diameter on the formation of borehole breakouts in black shale. Int J Rock Mech Min Sci 62:74–85. doi:10.1016/j.ijrmms.2013.03.012

Økland D, Cook JM (1998) Bedding-related borehole instability in high-angle wells. In: SPE/ISRM rock mechanics in petroleum engineering, 8–10 July, Trondheim, Norway. doi:10.2118/47285-MS

Ong SH, Roegiers J-C (1993) Influence of anisotropies in borehole stability. Int J Rock Mech Min Sci Geomech Abstr 30(7):1069–1075

Ong SH, Roegiers J-C (1996) Fracture initiation from inclined wellbores in anisotropic formations. J Pet Technol 612–619

Ottesen S (2010) Wellbore stability in fractured rock. In: IADC/SPE drilling conference and exhibition 128728, pp 1–8

Papamichos E, Tronvoll J, Skjærstein A, Unander TE (2010) Hole stability of Red Wildmoor sandstone under anisotropic stresses and sand production criterion. J Pet Sci Eng 72(1–2):78–92. doi:10.1016/j.petrol.2010.03.006

Pei J (2008) Strength of transversely isotropic rocks. Doctoral dissertation, Massachusetts Institute of Technology

Russell KA, Ayan C, Hart NJ, Rodriguez JM, Scholey H, Sugden C, Davidson JK (2003) Predicting and preventing wellbore instability using the latest drilling and logging technologies: Tullich Field Development, North Sea. In: SPE annual technical conference and exhibition, 5–8 October, Denver, Colorado. doi:10.2118/84269-MS

Skelton J, Hogg TW, Cross R, Verheggen L (1995) Case history of directional drilling in the Cusiana Field in Colombia. In: SPE/IADC drilling conference, Amsterdam, Netherlands. doi:10.2118/29380-MS

Vernik L, Liu X (1997) Velocity anisotropy in shales; a petrophysical study. Geophysics 62(2):521–532

Vernik L, Zoback MD (1990) Strength anisotropy in crystalline rock: implications for assessment of in situ stresses from wellbore breakouts. In: The 31th US symposium on rock mechanics (USRMS), 18–20 June, Golden, Colorado, pp 841–848

Wenk H-R, Voltolini M, Kern H, Popp T, Mazurek M (2008) Anisotropy in shale from Mont Terri. Lead Edge 2:742–748

Willson SM, Last NC, Zoback MD, Moos D (1999) Drilling in South America: a wellbore stability approach for complex geologic conditions. In: Latin American and Caribbean petroleum engineering conference, 21–23 April, Caracas, Venezuela. doi:10.2118/53940-MS

Zoback MD (2010) Reservoir geomechanics. Geophysics. Cambridge University Press, Cambridge